# Modeling and Simulation of Radar Sensor Artifacts for Virtual Testing of Autonomous Driving

Martin Friedrich Holder, Clemens Linnhoff,
Philipp Rosenberger, Christoph Popp, Hermann Winner
*Technische Universität Darmstadt*
*Institute of Automotive Engineering (FZD)*
Darmstadt, Germany
{holder, linnhoff, rosenberger, popp, winner}@fzd.tu-darmstadt.de

***Abstract*—Automotive radar measurements are prone to noisy sensor readings due to artifacts, such as false detections, clutter, and aliasing. Simulation models of sensors that are deployed in virtual testing pipelines must demonstrate a high degree of fidelity. Capturing artifacts correctly can be seen as a criteria for the trustworthiness of the model. In this work, we outline a comprehensive overview of different types of artifacts in radar along with their characteristics. Next, we allocate their formation process in the radar signal processing chain from which we draw implications about their correct modeling. We also present mathematical models that describe the artifacts along with their implementation in a radar simulation model.**

***Index Terms*—Radar Sensor Model, Autonomous Driving, Virtual Validation**

## I. Introduction

Virtual testing of autonomous driving requires simulation models of perception sensors, which include radar, camera, lidar, and ultrasonic. While being seen as a key sensor for autonomous driving, unprocessed radar sensor measurements are initially difficult to interpret. Prominent examples that appear frequently in radar include mirror reflections and measurement errors caused by limited resolution, clutter, and aliasing. This paper generalizes such effects as measurement artifacts that occur inherently in radar due to the underlying physical measurement principle, sensor performance characteristics, and wave propagation phenomena. The task of sensor modeling is understood as derivation of mathematical models of a sensor's measurement principle and sensor simulation can be seen as synthesizing (i.e. rendering) sensor measurements from a virtual scene. Therefore, meaningful virtual testing requires that the radar's sensing characteristics are captured precisely in a sensor model. In this paper, we are interested in studying different kinds of mechanisms that cause heterogeneous types of errors in the measurements of a radar sensor, along with their characteristic properties. The paper is organized as follows: First, the term *artifacts* is defined and different categories are exemplified with radar signal processing theory and observations from real world measurements. The second part contextualizes the derived categories of artifacts in the radar signal processing pipeline and discusses a comprehensive sensor data modeling level where all artifacts are captured. Here, the focus lies on deriving a data level suitable for modeling, that comprises all derived categories of artifacts and the integration into the recently reported Fourier tracing approach [1] is demonstrated. Lastly, it is shown how sensor artifacts are implemented in a radar sensor simulation model.

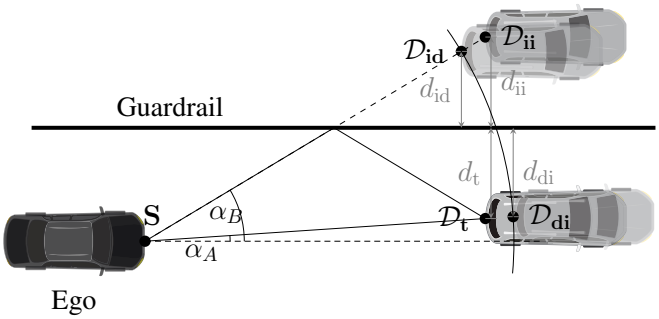


Fig. 1: Three cases of false detections originating from reflections of off guardrails. The actual target vehicle $\mathcal{D}_{\mathbf{T}}$ spawns three mirror detections, $\mathcal{D}_{\mathbf{id}}$, $\mathcal{D}_{\mathbf{ii}}$ and $\mathcal{D}_{\mathbf{di}}$ that are caused due to indirect-direct (id), indirect-indirect (ii), and direct-indirect (di) propagation.

## II. Artifacts in Radar and their Characteristics

Initially, the occurrence of a measurement error such as a mirror reflection is labeled as *false target* of false-positive or false-negative type. We expand the notation of *false target* as a more general result of unavoidable distortions in radar measurements, for which we define an artifact as follows:

**Definition** (Radar Artifact)**.** An *artifact* in a radar measurement is a noticeable distortion in the sensor readings that is unavoidable by the sensor measurement principle and its system design.

Due to their distinct similarities, discrimination of artifact detections[1] against real and relevant detections is difficult and makes correctly interpreting radar sensor readings within one measurement cycle a challenging task.

In particular those artifacts, which are linked to ambiguousness, do cause false measurements in cases where the correct hypothesis can no longer be inferred from the available data.

[1]Unless stated otherwise, we use the term *detection* for referring to a single measurement point that is reported from the radar and *target* to denote the actual, relevant object.

Following the definition above, six categories of artifacts that inherently differ in their physical origin are derived. While artifact categories are distinguishable from one another, they require unique approaches for their correct modeling.

### A. Mirror Reflections

With respect to their reflection properties for mm-wavelength in automotive radar, many surfaces are known to cause mirror reflections and settle false detections.When radar waves propagate, they can reflect off of pavement, road infrastructure (e.g. guardrails), or traffic participants, including the ego vehicle. This so-called multipath propagation alters the measurements of a radar. Multipath propagation is well studied for the two-dimensional case under the assumption of quasi-optical radar wave behavior [2], [3] and automated detection schemes are exist [3], [4]. Four feasible combinations of direct and indirect paths exist, three of which produce false-positive detections. These are illustrated in figure 1. In the depicted setup the detections $\mathcal{D}_{\text{id}}$ and $\mathcal{D}_{\text{di}}$ share the same radial distance to the sensor, but mirror detections show different lateral distances to the sensor $\mathbf{S}$, i.e. $d_{\text{id}} < d_{\text{di}}$, $d_{\text{di}} < d_{\text{t}}$, and $d_{\text{ii}} = d_{\text{t}}$.

Multipath propagation in three dimensions considers for example reflections off of pavement and guardrails and renders in this case five additional propagation paths, each causing multiple instances of (false-positive) detections. Extending the number of reflective surfaces, for instance when in a tunnel, additional cases are produced. The ego vehicle may also be seen as a reflecting surface and therefore as a potential source for repeated reflections (i.e. the wave, reflected off of the target vehicle, reflects off of the ego vehicle, bounces to the target, and back to the sensor).

Multipath reflections affect velocity measurements in addition to distance measurements. Recall that the Doppler frequency $f_{\text{D}}$ is proportional to the temporal change of a signal's path length between sender and receiver, denoted as $\ell_{\text{Tx,Rx}}$:

$$f_{\text{D}} \propto \frac{d\ell_{\text{Tx,Rx}}}{dt}. \tag{1}$$

A distortion of the relative velocity assigned to a detection, measured by Doppler shift, occurs when there is a difference in the time derivatives of the direct and indirect path length.

### B. Aliasing

The sampling theorem in radar sensors with widespread chirp-sequence modulation requires very high data rates that put high demands on the computational resources for data processing. Therefore, in practical radar system design, one relaxes the sampling theorem at the cost of introducing aliasing effects, leading to ambiguous measurements in angle and relative velocity. Prominent countermeasures to their elimination include resolution during tracking [5] and the observation of sequential ambiguous measurements [6]. Neither method can guarantee a correct resolution; any unresolved ambiguities remain as artifacts.

*1) Relative Velocity:* For obtaining the (radial) velocity of detections in chirp-sequence modulation, a fast Fourier transform (FFT) along each chirp is calculated and a second FFT operating over the sequence of all chirps produces phase information proportional to the relative velocity in radial direction. For unambiguous information, the maximum phase shift cannot exceed $\pi$, resulting in a maximum unambiguous Doppler measurement range of $\lambda/4\Delta t_{\text{ch}}$, where $\lambda$ and $\Delta t_{\text{ch}}$ indicate the wavelength and duration between each chirp. Because large unambiguous measurement ranges would require overlong measurement times, variable chirp repetition frequencies [7] or multiple frequency shift keying modulation [8] bypass this problem. Both methods require a set of subsequent measurements to resolve ambiguities, such that a single measurement is meaningless.

*2) Angular Measurement:* Although the maximum measurable azimuth angle is $\pi$ for an antenna array consisting of at least two patch antennas, the array's resolution and unambiguous measurement interval remain as design parameters. Maximizing both requires large aperture sizes with small spacing between antenna elements. Compact antenna designs are desirable for packaging reasons, but come at the expense of introducing ambiguities in the angular measurement. Similar to the relative velocity, aliasing effects occur when the angle extends the maximum unambiguously measurable angle, as outlined in [9].

### C. Limitation of resolution

All sensors have limited accuracy. A radar's measurement resolution is limited by the modulation bandwidth, antenna design, and measurement time as well as the window functions in the FFTs, see [7]. Obtaining range, range-rate, and azimuth angle with a radar is essentially the problem of estimating peak-frequencies in the periodogram. Its resolution limits translate directly to the corresponding resolution limits for range, radial velocity, and angle and are given in table I:

TABLE I: Radar resolution parameters and unambiguous measurement intervals

| | Range $r$ | Range rate $\dot{r}$ | Sine of azimuth $\phi$ |
|---|---|---|---|
| Resolution cell | $\Delta r = \frac{\text{c}}{2\Delta f_{\text{eff}}}$ | $\Delta \dot{r} = \frac{\lambda}{2T_{\text{M}}}$ | $\Delta \sin\phi = \frac{1}{I_\Phi \Delta\Gamma}$ |
| Unambiguous interval | $\left(0, \frac{\text{c}I_{\text{r}}}{2\Delta f_{\text{eff}}}\right)$ | $\left(\frac{-\lambda}{4\Delta t_{\text{ch}}}, \frac{\lambda}{4\Delta t_{\text{ch}}}\right)$ | $\left(\frac{-1}{2\Delta\Gamma}, \frac{1}{2\Delta\Gamma}\right)$ |

It can be seen that resolution parameters are dictated by the system design of the radar, such as modulation bandwidth $\Delta f_{\text{eff}}$, measurement time $T_{\text{M}}$, and number of antennas $I_\Phi$ with spacing $\Delta\Gamma$ normalized w.r.t. the wavelength. c denotes speed of light, and $I_{\text{r}}$ the number of sampling points per chirp. As a result of limited resolution, the measurements will show inaccuracies. An obvious case of an artifact caused by limited resolution occurs when multiple targets are located within one resolution cell. They are not separable in the data and appear as one detection. Another example for a limited resolution artifact is an incorrect height estimate by a radar sensor that does not measure elevation angle. This causes traversable objects,

such as bridges crossing the street or highly reflective objects on the ground, such as manhole covers, to be regarded as obstacles in the measuring plane. The overall limitation of the resolutions can be partially improved by approaches to high-resolution frequency estimation [10] and by obtaining additional information by observing the received signal over time [11].

### *D. Clutter / Measurement Noise*

Clutter detections occur when the detection threshold is randomly exceeded, but such detections are not associated with persistent targets. In addition to spurious, weak reflections from the terrain, electronic noise in the sensor can cause spontaneous detections that settle as clutter. Earlier work reported that the occurrence of clutter is well described by a Poisson distribution [12]. However, while clutter is primarily associated with unwanted detections and can initially be assumed to be noise, it has been shown that the information transmitted in terrain disturbances can be used for mapping and localization purposes [13].

### *E. Non-ideal signal processing*

Non-ideal behavior of high frequency (HF) components can causes adulteration of measurements. Artifacts of this kind are characterized by a dedicated formation process which justifies a separate category. Examples are nonlinearities in the electronic components as well as phase noise. Consider the mixer in the radar, that is often realized with Schottky diodes. The mixed signal can be found after a Taylor series expansion: While higher frequency components are suppressed by low-pass filters, the harmonics of the mixed signal's product can cause distractions if its attenuation is not sufficiently high. As a consequence, for a large and highly reflective target the radar will report a second target at the double distance, similar to a repeated path reflection, i.e. double reflection at the ego vehicle. In chirp sequence modulation, the frequency chirp ramps are assumed as perfectly linear. Nonlinearities will cause a widening of the range peaks proportional to the respective range bins. Phase noise results in a widening of spectral peaks and therefore, a less accurate estimate of the peak position. FMCW radars can influence each other due to interference [14]. The resulting false targets are also allocated to signal processing and methods for detection and mitigation exist [15], [16].

### *F. Object tracking artifacts*

Object tracking is the task of continuously estimating target states based on (noisy) sensor readings. Tracking filters often consume single detections that are combined into objects. The object list reported by automotive radar sensors includes filtering procedures, i.e. removing unwanted measurements and estimating the movement of targets. Tracking filters such as Kalman filters calculate estimates of target motion based on probability functions derived from measurements. They are based on assumptions about sensor measurements that are formalized in hypothesis and tracked over time. Temporal data aggregation allows for more accurate state estimates to be calculated rather than using a single measurement. In particular, during transient phases of the filter, where objects are spawning or disappearing, its state estimate has high variance and cannot be considered trustworthy. The gradual exchange of measurement information with estimation information causes the output of tracking filters to only partially reflect actual sensor measurements. Therefore, false-positive and false-negative information reported by object tracking filters exemplify a separate category of artifacts. Sensor fusion procedures at the object level typically aim to combine available measurements from several sensors in such a way that the respective state or existence uncertainty is minimized [17]. Figure 2 depicts object trajectories observed during traveling for approx. 1.8 km on a motorway.

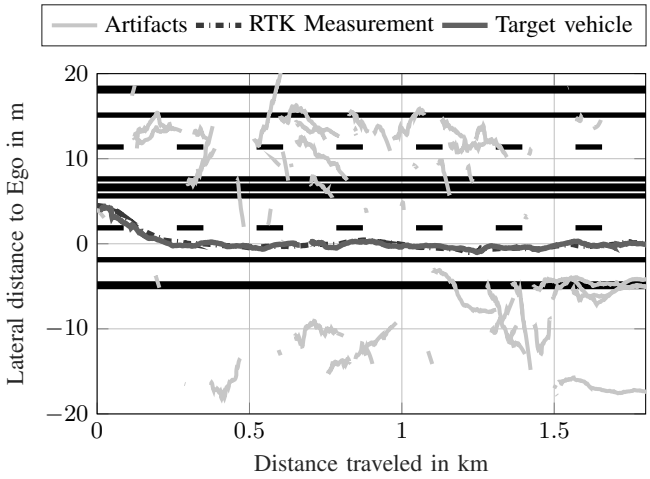


Fig. 2: Trajectory of a target vehicle and the associated object tracking artifacts that were observed while driving on the motorway. A few appear geometrically correct on the topmost lane (mirror reflection off of guardrail), others do not.

The trajectory of the target vehicle is obtained with RTK level accuracy (i.e. < 5 cm). When driving along the motorway, which consists of two lanes with railings on each side in light traffic, it can be seen that the target vehicle produces a series of other objects marked *artifacts* in the figure. Mirror objects occasionally appear in their geometrically correct position on the topmost track, but a number of objects exhibit incorrect behavior, with counter intuitive trajectories characterized by abrupt interruption. This is due to how the tracker combines available measurements in a way that satisfies certain hypotheses about object motion. Once an updated measurement no longer meets the assumptions under the selected hypothesis, it disappears. However, no statement can be made as to whether the target is principally rendered in the measurement and only the tracker discards it.

## III. Contextualizing Artifacts in the Radar Signal Processing Pipeline

The artifacts shown differ both in their physical origin and in their appearance in the measurements. This section

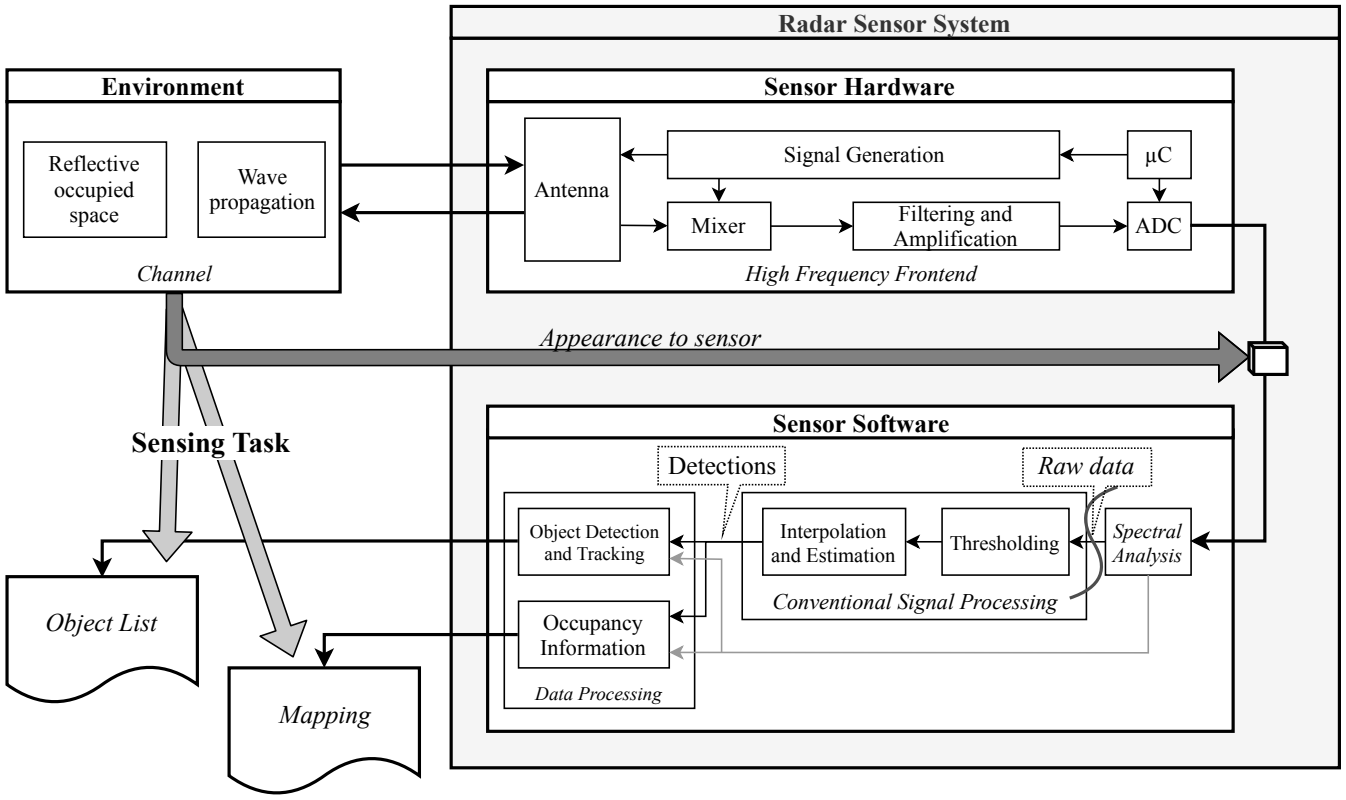


Fig. 3: Overview of a typical radar signal processing chain. The appearance of the channel is captured in the output data of the ADC. After spectral analysis and prior to thresholding, *raw* sensor data is available. Further signal processing generates single detections that are processed by algorithm, depending on the sensing task at hand. The figure shows the data processing chain for an object list and mapping, but other applications for radar data are also possible.

contextualizes artifacts in the radar signal processing pipeline, which is illustrated in figure 3. A radar sensor system consists of the sensor hardware and the sensor software components. The hardware part of the radar comprises the HF (high frequency) frontend, which contains the antenna as well as analog components for signal generation. The software part processes the digital signal that is available after the ADC (analog-to-digital converter). As already mentioned, the spectral analysis, which consists of subsequent FFTs, calculates the range-doppler-beam spectrum. In conventional signal processing, adaptive threshold algorithms, often variants of the CFAR algorithm, are now applied to the spectral data and peak values can be further processed to higher resolutions by interpolation or estimation. The so-called *detections* are now fed into the algorithm intended for the sensor task, such as object detection and tracking or occupancy estimation. Recently, algorithms that are applied to non-threshold data have been introduced and aim to be more robust against false-negative measurements and are presented for object tracking [18] and occupancy inference [19].

At this point, three observations are made: First, it can be seen that the appearance of a particular scenery (called *channel*) to the radar is fully conveyed in the signal that is available from the ADC. The spectral analysis allows for transforming the signal into physically meaningful spectral data with frequency resolutions according to table I. Second, all artifacts other than tracking artifacts can be found in the spectral data because their physical origin is in earlier processing steps. For example, there is a clear correlation between mirror detections and wave propagation as well as limited resolution and sensor hardware (e.g. antenna or modulation parameters). Third, the application of a detection threshold and interpolation/estimation algorithms has an irreversible character, as measured information is either removed or replaced by estimated information. In both cases one cannot distinguish between an artifact that was already present in the *raw data* and one introduced by interpolation and estimation calculations. Motivated by the fact that the (spectral) data prior to a threshold conveys (spectral) power values at a bin level in each measurement dimension, raw data contains the most comprehensive level of measured information. By capturing all presented categories of artifacts, except tracking artefacts, it is considered as the raw data interface in a radar sensor and as its corresponding simulation model. Therefore, we define *raw data* as follows:

**Definition** (Raw Data)**.** Raw data is a lossless representation of machine-interpretable and physical meaningful sensor readings. It is required that unambiguous (non-aliased) sensor readings in at least one physical domain can be calculated, based on a finite set of subsequent raw sensor data samples along with knowledge about additional sensor parameters. Raw data is exposed to artifacts in the respective sensor technology.

In the radar literature, the term *raw data* has several interpretations: It is often regarded as single detections, or targets (these two terms are often used synonymously to each other) that are available after the application of an adaptive threshold value to the power spectra. In this context, it serves as a counterpart to a point cloud in lidar sensors with relative velocity as additional information in each measurement data point. This type of data is also referred to as target lists [12], [20]–[22], radar detections [23], [24], and radar point clouds [25]. Additionally, the terms *feature data* [26], [27] as well as *low level data* [28], [29] are used in the context of sensor fusion. The latter emphasizes that no feature extraction from *raw data* is performed, but leaves it unclear to what extent data rate reduction (e.g. thresholding), interpolation, or ambiguity resolution has been performed. It can no longer be guaranteed that information that is required for correctly handling artifacts, such as resolving ambiguities, is still available. In conclusion, after application of a threshold, data does no longer qualify as *raw data*, because of the information loss.

## IV. Modeling

There are two methods for modeling the presented artifacts, either phenomenological or causal (also called *physical* modeling approach). The former is usually based on heuristics, which are enriched by findings from the observation of real measurements, from which physical laws are deduced. The effect of an artifact (e.g. a mirror object) can easily be added to synthetic data and the response of the system under test can be evaluated. For example, a mirror object caused by the presence of guardrails can be realized either by a trigger logic formalized in fixed rules ("if there is a guard rail in the visible area, you create mirror detections taking into account the current geometric conditions."). This method is computationally inexpensive, but is limited to applications where the interest is to study the behavior of the sensor signal and data processing pipeline or the function during the presence of a particular artifact. Artifacts generated by such hand-crafted rules may only have a limited degree of physical correctness and hypotheses that build upon plausibility checks can easily distinguish synthetic data from such a sensor model.

In a causal modeling approach, the goal is to implement the actual process of artifact development into the sensor model. It shows its strength in the ability to scale to complex virtual scenes and simultaneously render artifacts mathematically and physically correct. However, it increases the complexity of the sensor model: For example, the virtual world needs to comprise greater richness of detail in terms of material assignments for correctly calculating reflection paths. Also, more insight into the sensor hardware (e.g. resolution parameters) is required. Artifacts that are linked to the software (such as tracking artifacts) are naturally captured in the algorithm itself and show up as a consequence of the consumed data. Therefore, they do not require dedicated modeling steps as the algorithm will ideally show the same behavior when stimulated with real or synthetic data. In the following, we focus on modeling of artifacts due to mirror reflections and limitation of resolution and briefly discuss clutter detections and noise.

### A. Mirror reflections: Doppler alteration

Consider the scenario illustrated in figure 4.

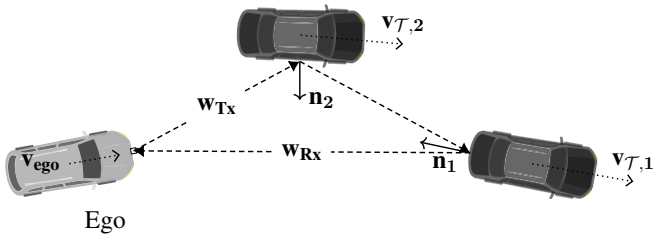


Fig. 4: Multitarget scenario under multipath propagation where each object travels with a different velocity.

The relative velocity from the ego vehicle's perspective that is obtained at the sensor reads:

$$\tilde{v}_{\text{rel,ego}} = \frac{1}{2}\mathbf{v}_{\text{ego}}\mathbf{w}_{\text{Rx}} + \frac{1}{2}\mathbf{v}_{\text{ego}}\mathbf{w}_{\text{Tx}} + \sum_{i=1}^{k_\text{i}} \mathbf{v}_{\mathcal{T},\text{i}} \cdot \mathbf{n}_\text{i} \qquad (2)$$

where $\mathbf{w}$ refers to the directions of the propagation paths for transmission and reception at the ego vehicle. $\mathbf{v}_{\mathcal{T},\text{i}}$ is the speed vector of the respective target $\mathcal{T}$ and $\mathbf{n}_i$ is the normal vector at an incident surface $i$, of which a total of $k_\text{i}$ interactions exist on the path between sender and receiver. Quantities accented with ~ denote simulated or calculated quantities. Note that $\mathbf{n}$ is the normal vector on a surface and corresponds to the bisectrix between the incidence and emergent angle. For the two-dimensional case with indirect-indirect signal path (see figure 1), the temporal change in path length causes the relative velocity w.r.t. to the ego vehicle of the mirror detection under incident angle $\alpha$ (assuming pure horizontal reflections) as

$$\tilde{v}_{\text{rel,ego}} = \cos(\alpha) \cdot (v_{\text{ego}} - v_{\mathcal{T}})\,. \qquad (3)$$

In case of direct-indirect signal path and vice versa, the relative velocity w.r.t. the ego vehicle reads

$$\tilde{v}_{\text{rel,ego}} = \frac{1}{2}\cos(\alpha) \cdot v_{\text{ego}} + \frac{1}{2}v_{\text{ego}} + \cos\left(\frac{\alpha}{2}\right) \cdot v_{\mathcal{T}}. \qquad (4)$$

The theory is briefly verified in a real-world measurement, where a target vehicle is followed by the ego vehicle with a radar sensor. Both cars are equipped with positioning devices at RTK level accuracy and travel on a two-lane motorway with a guardrail on the left side. Light traffic conditions allow to analyze the mirror detections that are spawned due to the presence of the guardrail over a time period of 3 s. Because the mirror detection appear on the left side, the receiving signal comes from an indirect path. Figure 5 displays the relative velocities for the real target and the mirror detections. In addition, the theoretical models for alteration of relative velocity under multipath (see eq. 4) for indirect-indirect (denoted as $v_{\text{rel,ii}}$ and indirect-direct $v_{\text{rel,id}}$) are shown.

It can be observed, that the mirror detections show a similar relative velocity which is in accordance to the indirect-indirect

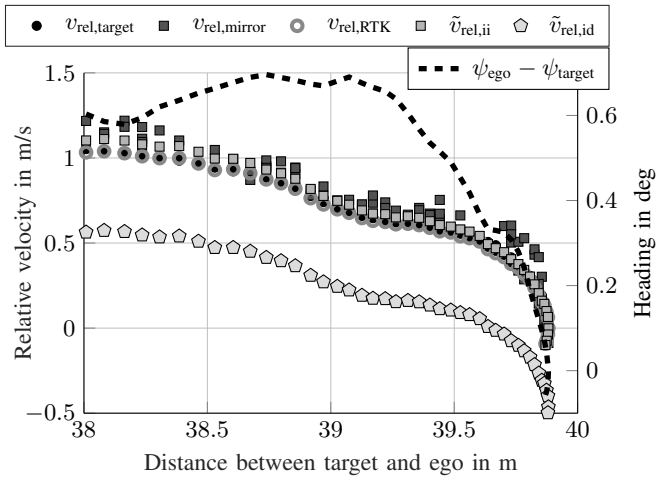


Fig. 5: Distribution of relative velocity measurements of a real target and mirror detections due to reflections off of a guardrail on a motorway.

model. The indirect-direct model, in contrast, shows less relative velocity for the mirror detections, that is not confirmed by the measurement. Deviations towards higher velocities of the mirror detections can be explained by sidewards reflections occurring at the target's spinning wheels that show different relative velocities compared to reflections off of the vehicle body. The heading angle $\psi$ is displayed for verification purposes and its variation of $< 1°$ justifies the assumption of a negligible lateral offset.

For studying the case of repeated reflection at the ego vehicle, a large truck is initially positioned in front of the radar-equipped ego car. In this configuration, eq. 4 would indicate that the relative velocity of the mirror detections would be double the actual relative velocity at double the distance, see figure 6a. The theory is well confirmed, as shown in figure 6b, where the real target can be seen around doppler bin 496. The mirror object is located at double the doppler counting down from 512 to 480. The number of range bins is also doubled. This artifact can further be replicated in synthesized data with Fourier tracing simulation, as depicted in figure 6c.

However, one has to note that verification by measurements of multipath propagation in higher dimensions poses a large challenge: In particular during dynamic scenes in real-world, influencing factors cannot be separated and propagation paths are exposed to a time-varying environment. This complicates extracting steady states for which the theory above holds.

### B. Aliasing

Modeling of aliasing effects is demonstrated for the Doppler domain. A radar varies the ramp duration between adjacent chirps within a measurement sequence ($\Delta t_{\text{ch}}$, see table I). In the studied scenario, the relative speed between the ego and the target vehicle exceeds the clear relative speed range. Consequently, the actual relative speed (which is > 100 km/h) can no longer be derived from a single measurement. This case is depicted in figure 7, comparing measurement and simulation

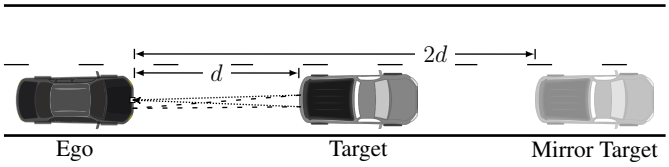


(a) Scenario setting: The wave bounces three times between ego and target before returning to the sensor.

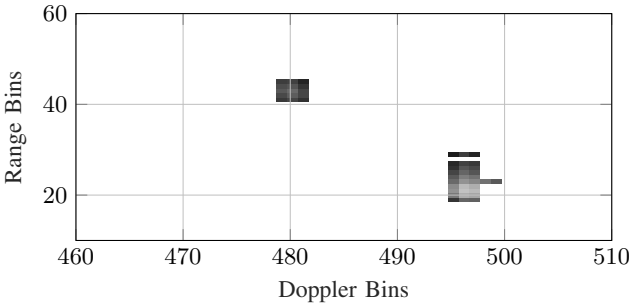


(b) Measured range Doppler map

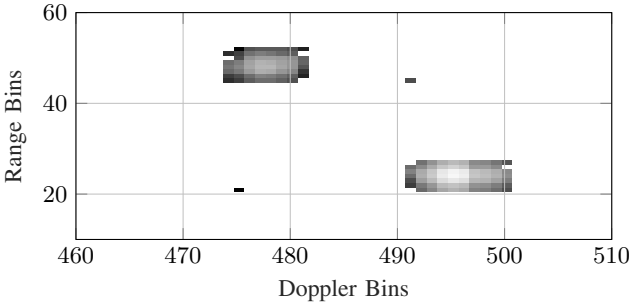


(c) Simulated range Doppler map

Fig. 6: Radar measurement and simulation of the double-reflection scenario. The mirror detections show double the relative velocity and double the range compared to the actual target.

results. The vertical line denotes the static return from the side strip and the detections appears as elliptically shaped entries around range-bin 90.

### C. Limitation of resolution

The vector-projection method [30] arose as a promising technique for modeling limited resolution in range, range rate, and azimuth. The key idea is to apply a smearing filter on a (sharp) reflection point, similar to a point spread function. In a previous work by the authors, the Fourier tracing approach [1], which builds on this principle, has demonstrated its ability to synthesize raw radar data from a virtual scene: With the resolution cells of the sensor as design parameters, artifacts associated with limited resolution and separability are realistically modeled with justifiable effort. A ray tracing engine approximates electromagnetic mm-waves under the assumption of geometric optics and facilitates the modeling of

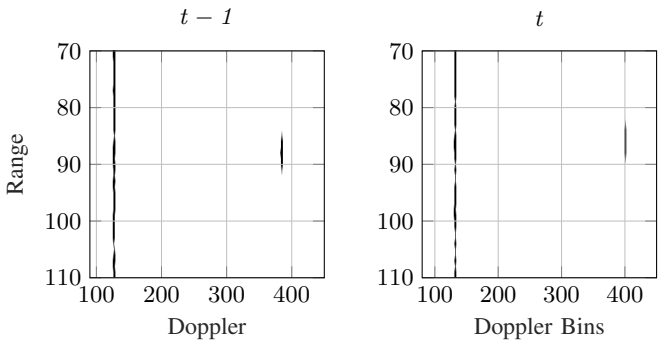


(a) Measured range Doppler map

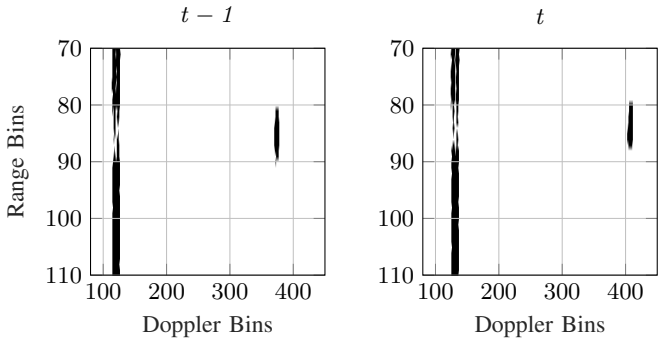


(b) Simulated range Doppler map

Fig. 7: Comparison of measurement and simulation at two consecutive time steps of a single target scenario that exceeds the unambiguous relative velocity interval.

artifacts related to wave propagation, such as mirror detections. Applying the Fourier scanning algorithm to elevated objects, such as bridges, generates apparently realistic results, see figure 8.

### *D. Clutter / Measurement Noise*

Recall that clutter is understood as a random detection, i.e. detections that are present in the current, but not in the previous measurement cycle. In an experiment, a radar is facing towards a *feature-poor* and all-static terrain. The grassland area is studied from five different positions (denoted Grassland 1 to 5). For reference, an additional measurement is carried out where the sensor observes a different area with a set of static objects, such as cars. Now, only range bins that have not been reported as occupied in the previous measurement cycle are studied. This allows to consider only non-persistent detections that may be considered as clutter. Figure 9 shows the distribution of the clutter detections and it shows the probability that at least one detection is reported for a range bin during a given period of time. In particular for higher range bins (larger distances from the radar), this probability may be well approximated by a uniform distribution. Therefore, suche clutter detections may be modeled as uniformly distributed peaks across the studied spectra.

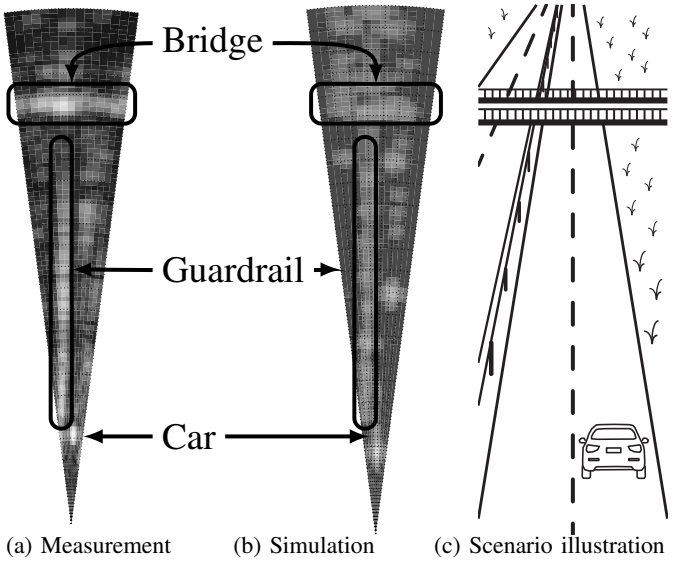


(a) Measurement (b) Simulation (c) Scenario illustration

Fig. 8: Measurement and simulation of a range-beam map of a scenario with a bridge representing an elevated object.

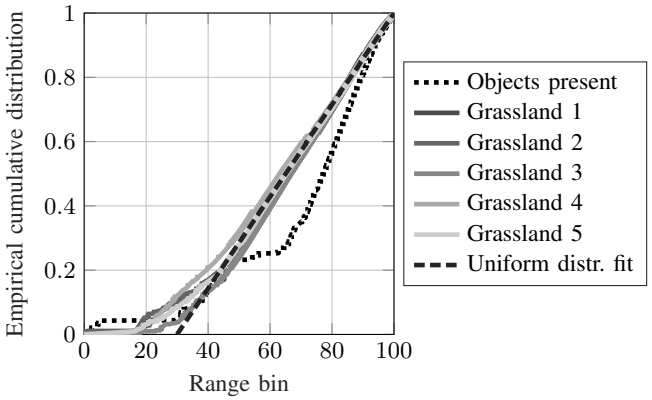


Fig. 9: Probability distribution of clutter detections in range bins during observing a static scenario for a period of time.

Measurement noise characteristics are investigated in an experiment in which cube corner reflectors of different sizes are positioned at distances between 15 m and 75 m in front of a radar. The stationary scenario was observed for a period of 60 s and the power values at the corresponding range bin, in which the cube corner is located, are investigated. A $\chi^2$ test with 5 % significance level shows that the distribution of power measures meets the assumption of a normal distribution as model for measurement noise for point targets, such as cube corner reflectors. It should be noted that this does not claim to describe amplitude variations of extended targets (e.g. cars) at different aspect angles. This phenomenon is investigated in earlier works of the authors [31].

## V. Conclusion

This paper presents a sound definition of different radar sensor artifacts and corresponding modeling approaches. Measurements showing various sensor artifacts were carried out

in real world test drives, as well as specially developed measurement campaigns on a test site. Mathematical models for artifacts are introduced and their explanatory power is proven by comparison with measurements. Simulations verify the correct implementation in a sensor model. It should be emphasized that the above list of artifacts does not claim to be exhaustive, but represents those artifacts which are most dominant and easy to observe in radar measurements. Therefore, it can be considered as the minimum set of effects that a reasonable radar sensor model should provide. We explicitly stress the fact that the occurrence of an artifact does not imply an unwanted measurement. For example, radar sensors are able to pick up reflections from occluded objects. These reflections fulfill our definition of artifacts, but provide additional information for a holistic understanding of the scene. Nevertheless, these reflections are also exposed to the distortions shown due to multipath propagation effects.

Further investigations will focus on a more detailed quantification of artifacts that are linked to non-ideal signal processing, as well as their corresponding modeling methods. The limits of the fidelity of the proposed modelling methods also need to be further examined. In safety validation with the scenario-based testing approach, a detailed notation of what revolves around the logical description of a scenario exist [32]. It lacks, however, consideration of machine perception related aspects in order to include sensor artifacts, as the ones presented in this paper. Further work should therefore focus on expanding the scenario description language with sensor specific aspects. The scenarios representing specified artifacts considered in this paper can serve as a starting point.

## REFERENCES


[1] M. Holder, C. Linnhoff, P. Rosenberger, and H. Winner, "The Fourier Tracing Approach for Modeling Automotive Radar Sensors," in *2019 20th International Radar Symposium (IRS)*. IEEE, Jun. 2019. [Online]. Available: https://doi.org/10.23919/irs.2019.8768113

[2] A. Kamann, P. Held, F. Perras, P. Zaumseil, T. Brandmeier, and U. T. Schwarz, "Automotive Radar Multipath Propagation in Uncertain Environments," in *2018 21st International Conference on Intelligent Transportation Systems (ITSC)*. IEEE, Nov. 2018. [Online]. Available: https://doi.org/10.1109/itsc.2018.8570016

[3] F. Roos, M. Sadeghi, J. Bechter, N. Appenrodt, J. Dickmann, and C. Waldschmidt, "Ghost target identification by analysis of the Doppler distribution in automotive scenarios," in *2017 18th International Radar Symposium (IRS)*. IEEE, Jun. 2017. [Online]. Available: https://doi.org/10.23919/irs.2017.8008128

[4] R. Prophet, J. Martinez, J.-C. F. Michel, R. Ebelt, I. Weber, and M. Vossiek, "Instantaneous Ghost Detection Identification in Automotive Scenarios," in *2019 IEEE Radar Conference (RadarConf)*. IEEE, Apr. 2019. [Online]. Available: https://doi.org/10.1109/radar.2019.8835603

[5] K. Li, B. Habtemariam, R. Tharmarasa, M. Pelletier, and T. Kirubarjan, "Multitarget Tracking with Doppler Ambiguity," *IEEE Transactions on Aerospace and Electronic Systems*, vol. 49, no. 4, pp. 2640–2656, oct 2013. [Online]. Available: https://doi.org/10.1109/taes.2013.6621842

[6] N. Levanon, *Radar Signals*. Hoboken, New Jersey: John Wiley & Sons, Inc, 2004.

[7] H. Winner, "Automotive RADAR," in *Handbook of Driver Assistance Systems*. Springer International Publishing, Dec. 2015, pp. 325–403. [Online]. Available: https://doi.org/10.1007/978-3-319-12352-3_17

[8] M. Kronauge and H. Rohling, "New chirp sequence radar waveform," *IEEE Transactions on Aerospace and Electronic Systems*, vol. 50, no. 4, pp. 2870–2877, Oct. 2014. [Online]. Available: https://doi.org/10.1109/taes.2014.120813

[9] S. Rao, "Introduction to mmwave Sensing: FMCW Radars," https://training.ti.com/sites/default/files/docs/mmwaveSensing-FMCW-offlineviewing_0.pdf, 2017.

[10] F. Engels, P. Heidenreich, A. M. Zoubir, F. K. Jondral, and M. Wintermantel, "Advances in Automotive Radar: A framework on computationally efficient high-resolution frequency estimation," *IEEE Signal Processing Magazine*, vol. 34, no. 2, pp. 36–46, Mar. 2017. [Online]. Available: https://doi.org/10.1109/msp.2016.2637700

[11] F. Diewald, J. Klappstein, F. Sarholz, J. Dickmann, and K. Dietmayer, "Radar-interference-based bridge identification for collision avoidance systems," in *2011 IEEE Intelligent Vehicles Symposium (IV)*. IEEE, Jun. 2011. [Online]. Available: https://doi.org/10.1109/ivs.2011.5940422

[12] M. Bühren and B. Yang, "Simulation of Automotive Radar Target Lists considering Clutter and Limited Resolution," in *Proceedings of International Radar Symposium (IRS) 2007*, Cologne, Germany, Sep. 2007, pp. 195–200.

[13] M. Holder, S. Hellwig, and H. Winner, "Real-time pose graph SLAM based on radar," in *2019 IEEE Intelligent Vehicles Symposium (IV)*. IEEE, Jun. 2019. [Online]. Available: https://doi.org/10.1109/ivs.2019.8813841

[14] S. Alland, W. Stark, M. Ali, and M. Hegde, "Interference in automotive radar systems: Characteristics, mitigation techniques, and current and future research," *IEEE Signal Processing Magazine*, vol. 36, no. 5, pp. 45–59, Sep. 2019. [Online]. Available: https://doi.org/10.1109/msp.2019.2908214

[15] C. Fischer, H. L. Blocher, J. Dickmann, and W. Menzel, "Robust detection and mitigation of mutual interference in automotive radar," in *2015 16th International Radar Symposium (IRS)*. IEEE, Jun. 2015. [Online]. Available: https://doi.org/10.1109/irs.2015.7226239

[16] M. Barjenbruch, D. Kellner, K. Dietmayer, J. Klappstein, and J. Dickmann, "A method for interference cancellation in automotive radar," in *2015 IEEE MTT-S International Conference on Microwaves for Intelligent Mobility (ICMIM)*. IEEE, Apr. 2015. [Online]. Available: https://doi.org/10.1109/icmim.2015.7117925

[17] M. Munz, K. Dietmayer, and M. Mahlisch, "Generalized fusion of heterogeneous sensor measurements for multi target tracking," in *2010 13th International Conference on Information Fusion*. IEEE, Jul. 2010. [Online]. Available: https://doi.org/10.1109/icif.2010.5711926

[18] B. K. Habtemariam, R. Tharmarasa, and T. Kirubarajan, "PHD filter based track-before-detect for MIMO radars," *Signal Processing*, vol. 92, no. 3, pp. 667–678, Mar. 2012. [Online]. Available: https://doi.org/10.1016/j.sigpro.2011.09.007

[19] R. Weston, S. Cen, P. Newman, and I. Posner, "Probably Unknown: Deep Inverse Sensor Modelling Radar," in *2019 International Conference on Robotics and Automation (ICRA)*. IEEE, May 2019. [Online]. Available: https://doi.org/10.1109/icra.2019.8793263

[20] R. Prophet, M. Hoffmann, M. Vossiek, G. Li, and C. Sturm, "Parking space detection from a radar based target list," in *2017 IEEE MTT-S International Conference on Microwaves for Intelligent Mobility (ICMIM)*. IEEE, Mar. 2017. [Online]. Available: https://doi.org/10.1109/icmim.2017.7918864

[21] L. Stanislas and T. Peynot, "Characterisation of the Delphi Electronically Scanning Radar for robotics applications," in *Australasian Conference on Robotics and Automation (ACRA 2015)*, Canberra, A.C.T, December 2015. [Online]. Available: https://eprints.qut.edu.au/92567/

[22] J. Oh, K.-S. Kim, M. Park, and S. Kim, "A Comparative Study on Camera-Radar Calibration Methods," in *2018 15th International Conference on Control, Automation, Robotics and Vision (ICARCV)*. IEEE, Nov. 2018. [Online]. Available: https://doi.org/10.1109/icarcv.2018.8581329

[23] M. Li, Z. Feng, M. Stolz, M. Kunert, R. Henze, and F. Küçükay, "High Resolution Radar-based Occupancy Grid Mapping and Free Space Detection," in *VEHITS*, 2018, pp. 70–81.

[24] AutonomouStuff, "Delphi ESR V9.21.15 Radar," https://autonomoustuff.com/product/delphi-esr-9-21-15/, 2018, [Online; accessed 30-August-2019].

[25] O. Schumann, M. Hahn, J. Dickmann, and C. Wohler, "Semantic Segmentation on Radar Point Clouds," in *2018 21st International Conference on Information Fusion (FUSION)*. IEEE, Jul. 2018. [Online]. Available: https://doi.org/10.23919/icif.2018.8455344

[26] M. Serfling, *Merkmalsbasierte Fusion einer NIR-Kamera und eines bildgebenden Radarsensors zur Fußgängerwarnung bei Nacht*. Aachen: Shaker, 2011.

[27] N. Kämpchen, "Feature-level fusion of laser scanner and video data for advanced driver assistance systems," Ph.D. dissertation, Universität

Ulm, 2007. [Online]. Available: https://oparu.uni-ulm.de/xmlui/handle/123456789/409

[28] M. Haberjahn, "Multilevel Datenfusion konkurrierender Sensoren in der Fahrzeugumfelderfassung," Ph.D. dissertation, Humboldt-Universität zu Berlin, Mathematisch-Naturwissenschaftliche Fakultät II, 2013.

[29] R. Grover, G. Brooker, and H. F. Durrant-Whyte, "A low level fusion of millimeter wave radar and night-vision imaging for enhanced characterization of a cluttered environment," in *Proceedings 2001 Australian Conference on Robotics and Automation*, 2001.

[30] P. Cao, "Modeling Active Perception Sensors for Real-Time Virtual Validation of Automated Driving Systems," Ph.D. dissertation, Technische Universität, Darmstadt, July 2018. [Online]. Available: http://tuprints.ulb.tu-darmstadt.de/7539/

[31] M. Holder, P. Rosenberger, H. Winner *et al.*, "Measurements Revealing Challenges in Radar Sensor Modeling for Virtual Validation of Autonomous Driving," in *2018 21st International Conference on Intelligent Transportation Systems (ITSC)*. IEEE, Nov. 2018. [Online]. Available: https://doi.org/10.1109/itsc.2018.8569423

[32] J. Sauerbier, J. Bock, H. Weber, and L. Eckstein, "Definition of Scenarios for Safety Validation of Automated Driving Functions," *ATZ worldwide*, vol. 121, no. 1, pp. 42–45, dec 2018. [Online]. Available: https://doi.org/10.1007/s38311-018-0197-2